Supporting Information

Electrochemically Controlled Ion Dynamics in Porphyrin Nanostructures

Andrés F. Molina-Osorio,[†] José A. Manzanares,[‡] Alonso Gamero-Quijano[†] and Micheál D. Scanlon*[,†,§]

[†] The Bernal Institute and Department of Chemical Sciences, School of Natural Sciences, University of Limerick (UL), Limerick V94 T9PX, Ireland.
[‡] Department of Thermodynamics, Faculty of Physics, University of Valencia, c/Dr. Moliner, 50, E-46100 Burjasot, Spain.
[§] Advanced Materials and Bioengineering (AMBER) Centre, Ireland.

*E-mail: micheal.scanlon@ul.ie

Table of Contents

Section S1. Experimental Section

S1.1 Materials

All reagents were used as received without further purification. Zinc(II) 5,10,15,20-(tetra-4-carboxyphenyl)porphyrin (ZnPor, ≥ 98%) was purchased from Porphychem. All aqueous solutions were prepared with ultra-pure water (Millipore Milli-Q, resistivity 18.2 MΩ·cm). Bis(triphenylphosphoranylidene)ammonium chloride (R_2NCl, 97% with R = triphenylphosphoranylidene) and lithium tetrakis(pentafluorophenyl)borate diethyletherate ($[Li(OEt_2)]TB$) were obtained from Sigma-Aldrich and Boulder Scientific Company, respectively. Bis(triphenylphosphoranylidene)ammonium tetrakis(pentafluorophenyl)borate (R_2NTB) was prepared by metathesis of equimolar solutions of R_2NCl and $[Li(OEt_2)]TB$ in a methanol-water (2:1 v/v) mixture. The resulting precipitates were filtered, washed, recrystallised from acetone and finally washed 5 times with a methanol-water (2:1 v/v) mixture. Lithium chloride (LiCl, ≥ 99%), lithium hydroxide (LiOH, ≥ 98%), tetraethylammonium chloride (TEACl, ≥ 98%) and citric acid (H_3Cit, ≥ 99.5%) were obtained from Sigma-Aldrich. The organic solvent α,α,α-trifluorotoluene (TFT, ≥ 99%) was obtained from Acros Organics.

S1.2 Functionalising the liquid|liquid interface

Aqueous solutions of ZnPor were prepared by directly dissolving the solid in a lithium citrate (Li_2HCit) buffer pre-adjusted to the desired pH, followed by sonication of the solution for three minutes. Depending on the experiment, the concentration of ZnPor was varied in the range of 10 to 100 μM and the ionic strength of the Li_2HCit buffer solution was maintained at 10 (±2) mM. The selective formation of ZnPor nanostructures at the interface between water and TFT in the four-electrode electrochemical cell was observed upon contacting the ZnPor aqueous solution with the TFT electrolyte. As rationalised in detail recently,[1] self-assembly was observed only at pH = 5.8 = pK_a(COOH), where the ratio between neutral (fully protonated) and tetra-anionic species was close to 1. The self-assembly process was carried out at open circuit potential conditions for 30 min unless stated otherwise. To isolate the ZnPor-INs at the interface, as shown in Figure S1, the upper 50% of the volume of the aqueous phase was carefully removed by a pipette and replaced with porphyrin-free aqueous electrolyte. This procedure was repeated until no porphyrin was detectable in the aqueous phase by UV/vis spectroscopy.

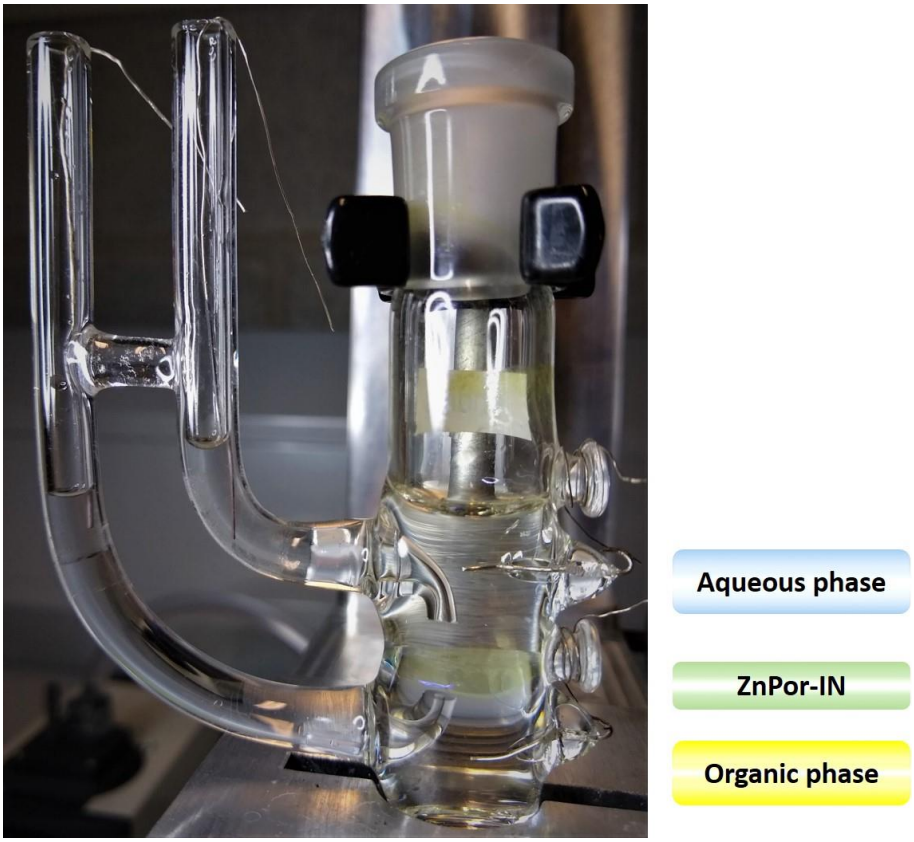

Figure S1. Image of a four-electrode electrochemical cell with the yellow/green ZnPor-IN film floating at the ITIES formed between a Li_2HCit buffered aqueous solution and an organic solution of R_2NTB in TFT (see Scheme 2, main text).

S1.3 Spectroscopic determination of the interfacial concentration Γ_{ZnPor} of ZnPor-INs

The surface concentration Γ_{ZnPor} of the ZnPor-IN was measured following a procedure described recently.[1] Vials containing biphasic systems of ZnPor in lithium citrate buffer (10 mM ionic strength, pH 5.8) at different initial concentrations [ZnPor] in the bulk aqueous phase, and 5 mM R_2NTB in TFT as the organic phase were prepared and left to stand for 30 min. After this time, the porphyrin not adsorbed at the interface was extracted and analysed by UV/vis absorbance spectroscopy to quantify the porphyrin concentration therein (final bulk concentration). By subtracting the final from the initial bulk concentrations, the surface concentration (number of moles adsorbed per geometric area of aqueous|organic interface) was determined. A linear relationship between Γ_{ZnPor} and [ZnPor] was observed as presented in Figure S2a. Quantification of [ZnPor] not adsorbed at the interface was performed using the calibration curve presented in Figure S2b.

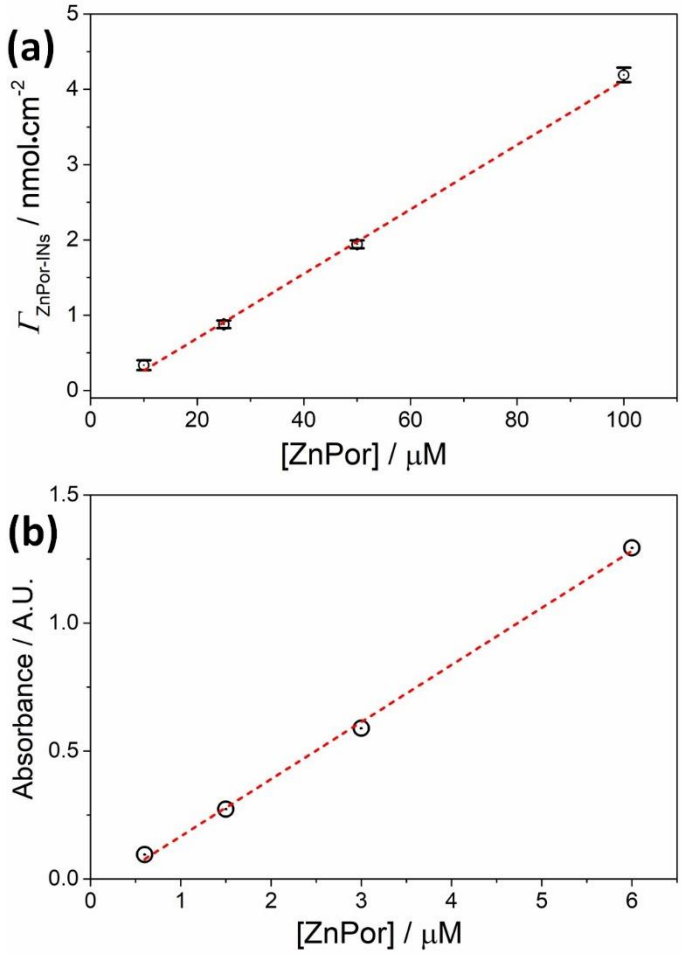

Figure S2. (a) Surface concentration Γ_{ZnPor} of ZnPor-INs as a function of ZnPor concentration [ZnPor] in the bulk aqueous phase. The surface concentration was measured after 30 min of ZnPor self-assembly at pH 5.8 as described in the Experimental Section. **(b)** UV/vis calibration curve used for the quantification of [ZnPor] not adsorbed at the interface. The absorbance was measured at λ_{max} = 422 nm.

S1.4 Electrochemical measurements

Electrochemical experiments at the ZnPor-IN functionalised water-TFT interface were performed using an Autolab PGSTAT204 potentiostat. The general configuration of the biphasic system were outlined in Scheme 2, main text. The four-electrode electrochemical cell had a geometric area of 1.87 cm^2. To supply the current flow, platinum counter electrodes were positioned in the organic and aqueous phases. The potential drop at the liquid|liquid interface was measured by means of a silver/silver citrate (Ag/AgCit) reference electrode immersed in the aqueous phase and a silver/silver chloride (Ag/AgCl) reference electrode immersed in the organic reference solution (an aqueous solution of 10 mM LiCl and 1 mM R_2NCl). Both

reference electrodes were connected to the aqueous phase and organic reference solution, respectively, through Luggin capillaries. The organic phase was composed of a highly hydrophobic salt R_2NTB, dissolved in TFT. The aqueous phase consisted of a Li_2HCit solution at different pH values. By introducing a salt in each phase, the interfacial Galvani potential difference $\Delta_o^w\phi$ was varied by external polarisation with a polarisable potential window ranging from –0.3 to +0.6 V. The voltammetry was adjusted to the Galvani potential scale by assuming the formal ion transfer potential of TEA^+ to be 0.149 V.[2]

Cyclic voltammetry and potential step chronoamperometry experiments were performed using *iR* drop compensation (1000 Ω). Differential capacitances at different applied voltages were measured using alternating current voltammetry, also known as potentiodynamic electrochemical impedance spectroscopy, at 80 Hz and assuming the cell behaves as a series R-C circuit. At this frequency, the contribution of Faradaic processes was significant only at the edge of the potential window.

Section S2. Electrochemistry of the floating film of ZnPor-INs at the ITIES

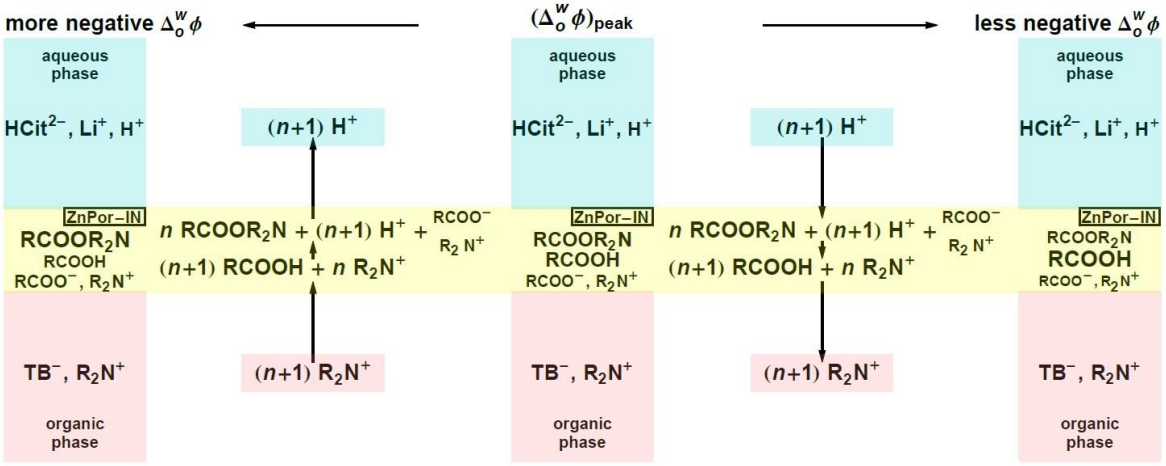

Scheme S1. Detailed schematic of the electrochemically-driven reversible ion intercalation process involving the ZnPor-IN film floating at the electrified liquid|liquid interface, as described in Scheme 1, main text.

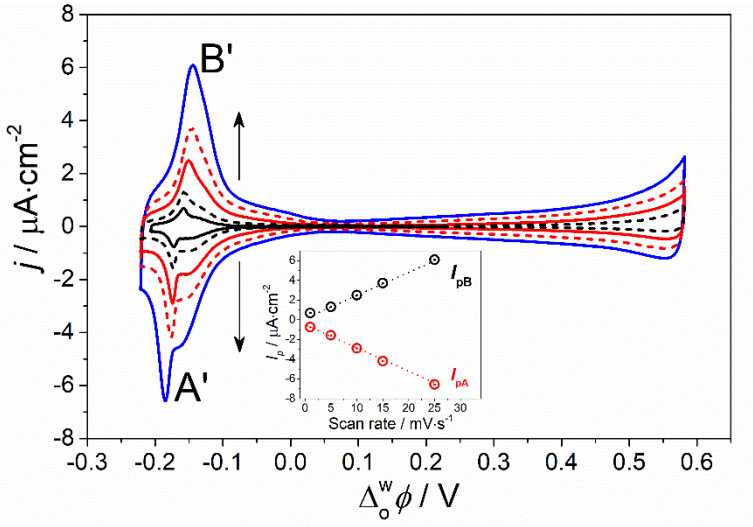

Figure S3. Effect of the scan rate on the electrochemical response of the ZnPor-IN film. The scan rates used were 1, 5, 10, 15 and 25 mV·s^{-1} and Γ_{ZnPor} was 0.34 nmol·cm^{-2}. The electrochemical configuration of the cell was as described in Scheme 2, main text. Inset: the peak current I_p dependence on the scan rate.

Table S1. Analysis of the voltammetric features observed in Figure S3.

Scan rate/(mV·s^{-1})	ΔE_p/mV	Q_A/Q_B
5	19	1.0
10	24	1.0
15	30	0.99
25	40	0.97
50	59	0.96

Table S2. Analysis of the voltammetric features observed in Figure 2b in the main manuscript (data obtained at a scan rate of 1 mV·s^{-1}).

Γ_{ZnPor}/(nmol·cm^{-2})	ΔE_p/mV	Q_A/Q_B
0.34	14	0.75
0.88	18	0.85
1.94	23	0.86
4.19	29	0.89

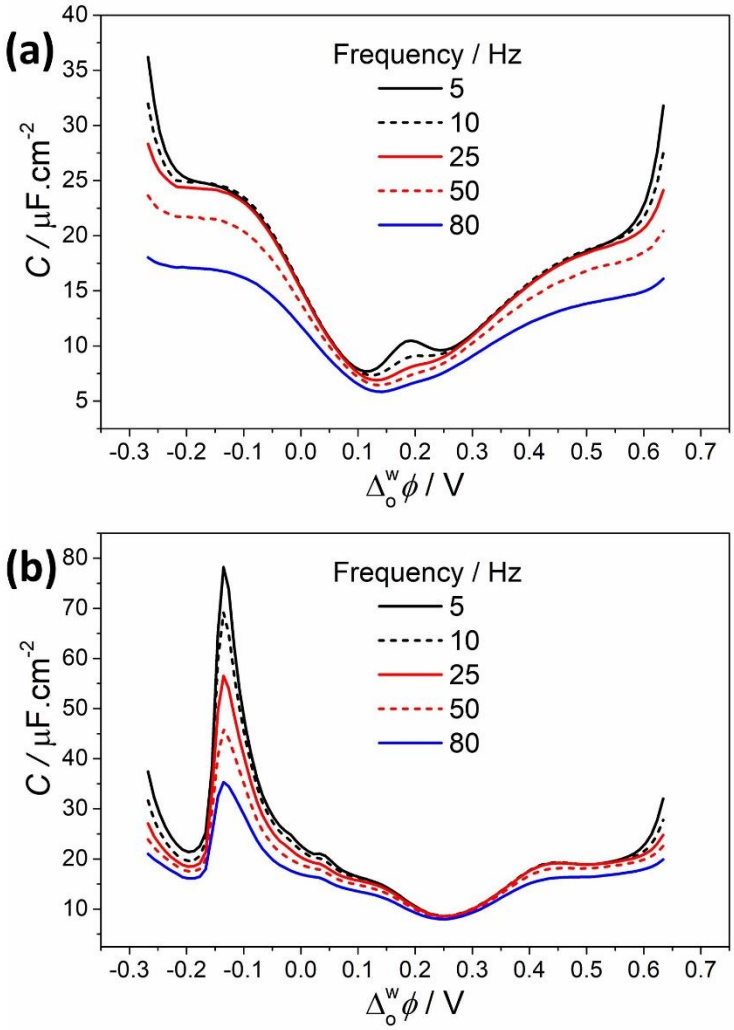

Figure S4. Differential capacitance curves at **(a)** the bare ITIES in the presence of 125 µM of TEACl and 10 mM LiH_2Cit at pH 5.8 in the aqueous phase and **(b)** the ITIES functionalised with a ZnPor-IN film. The capacitance was calculated from impedance measurements every 5 mV at different frequencies assuming an *RC* circuit where *R* represents the solution resistance and *C* the double layer capacitance. The electrochemical configuration of the cell was as described in Scheme 2, main text. Γ_{ZnPor} determined spectroscopically as 0.34 nmol·cm^{-2}.

Figure S4a demonstrates that at 80 Hz the contribution of Faradaic processes was significant only at the edge of the potential window, with the Faradaic ion transfer response of TEA^+ ion transfer entirely filtered out. Meanwhile, in Figure S4b, the peak observed at –0.15 V in the presence of the ZnPor-IN remains, indicating that the latter are associated with adsorption and capacitive processes.

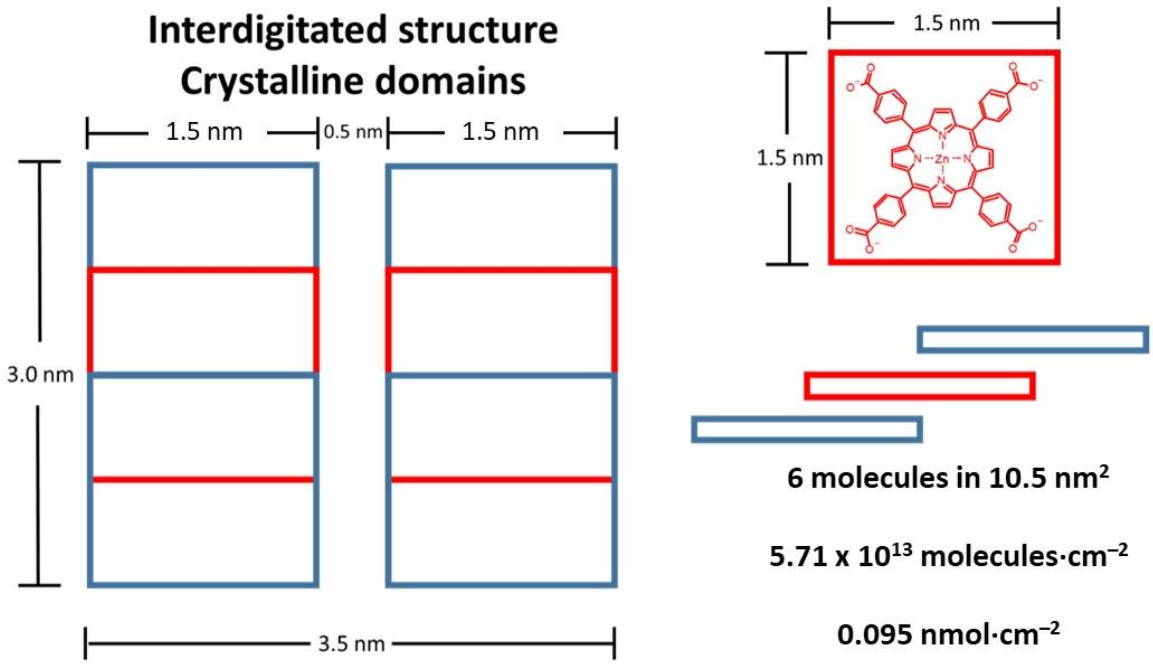

Figure S5. The interdigitated clathrate structure was recently obtained from the XRD analysis of the ZnPor-IN film.[1] The area of a single ZnTPPc molecule is 2.25 nm^2.[3]Assuming perfectly flat lying ZnTPPc molecules in a monolayer and fully crystalline domains of ZnPor-INs in contact with the liquid|liquid interface (*i.e.*, no amorphous domains), the theoretical monolayer concentration of the ZnPor-INs was calculated as $\Gamma_m = 0.095\ nmol \cdot cm^{-2}$ (equivalent to $5.71 \times 10^{13}\ molecules \cdot cm^{-2}$).

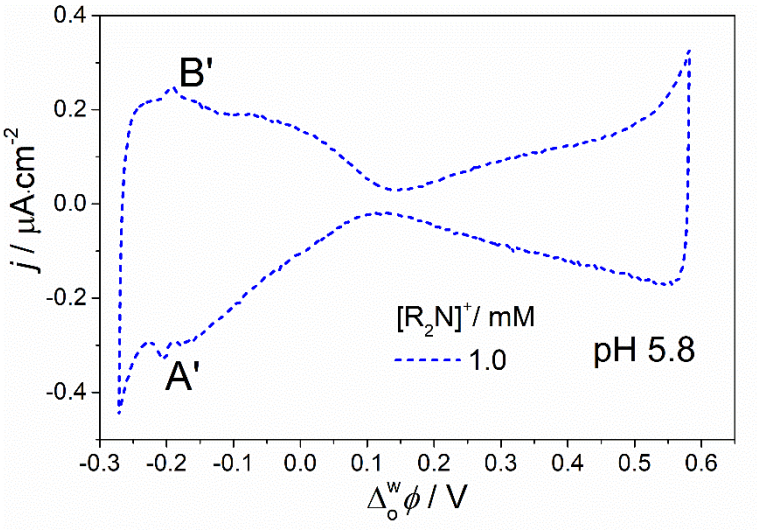

Figure S6. Zoomed version of the CV obtained with $[R_2N^+]$ = 1 mM (dashed blue line in Figure 2d, main text). The scan rate was 5 mV·s^{-1} and Γ_{ZnPor} was 0.34 nmol·cm^{-2}.

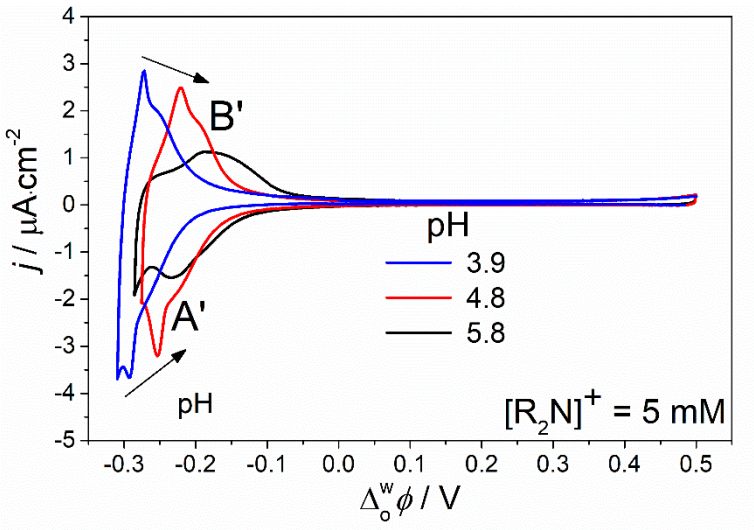

Figure S7. The effect of pH on the electrochemical response was also investigated when the aqueous anion was changed from citrate to chloride. The cell configuration was as described in Scheme 2, main text, with LiCl replacing Li_2HCit. The scan rate was 5 mV·s^{-1} and Γ_{ZnPor} was 0.34 nmol·cm^{-2}.

Section S3. Modelling the electrochemistry of the floating film of ZnPor-INs at the ITIES

S3.1 Distribution equilibrium of the ionic species between phase IN and their bulk phases

The distribution equilibria of the ionic species R_2N^+, TB^-, $HCit^{2-}$, H^+ and Li^+ between phase IN and their respective bulk phases are given by the equality of their electrochemical potentials in these phases, $\tilde{\mu}^{\mathrm{o}}_{\mathrm{R_2N}} = \tilde{\mu}^{\mathrm{IN}}_{\mathrm{R_2N}}$, $\tilde{\mu}^{\mathrm{o}}_{\mathrm{TB}} = \tilde{\mu}^{\mathrm{IN}}_{\mathrm{TB}}$, $\tilde{\mu}^{\mathrm{w}}_{\mathrm{HCit}} = \tilde{\mu}^{\mathrm{IN}}_{\mathrm{HCit}}$, $\tilde{\mu}^{\mathrm{w}}_{\mathrm{Li}} = \tilde{\mu}^{\mathrm{IN}}_{\mathrm{Li}}$ and $\tilde{\mu}^{\mathrm{w}}_{\mathrm{H}} = \tilde{\mu}^{\mathrm{IN}}_{\mathrm{H}}$. Thus, their concentrations in phase IN can be written as

$$c^{\mathrm{IN}}_{\mathrm{R_2N}} = c^{\mathrm{o,b}} P_{\mathrm{R_2N}} \mathrm{e}^{-f\Delta^{\mathrm{IN}}_{\mathrm{o}}\phi} \quad \text{(S1)}$$

$$c^{\mathrm{IN}}_{\mathrm{TB}} = c^{\mathrm{o,b}} P_{\mathrm{TB}} \mathrm{e}^{f\Delta^{\mathrm{IN}}_{\mathrm{o}}\phi} \quad \text{(S2)}$$

$$c^{\mathrm{IN}}_{\mathrm{HCit}} = c^{\mathrm{w,b}} P_{\mathrm{HCit}} \mathrm{e}^{-2f\Delta^{\mathrm{w}}_{\mathrm{IN}}\phi} \quad \text{(S3)}$$

$$c^{\mathrm{IN}}_{\mathrm{H}} = c^{\mathrm{w,b}}_{\mathrm{H}} P_{\mathrm{H}} \mathrm{e}^{f\Delta^{\mathrm{w}}_{\mathrm{IN}}\phi} \quad \text{(S4)}$$

$$c^{\mathrm{IN}}_{\mathrm{Li}} = \left(2c^{\mathrm{w,b}} - c^{\mathrm{w,b}}_{\mathrm{H}}\right) P_{\mathrm{Li}} \mathrm{e}^{f\Delta^{\mathrm{w}}_{\mathrm{IN}}\phi} \quad \text{(S5)}$$

where $c^{\mathrm{o,b}} = c^{\mathrm{o,b}}_{\mathrm{R_2N}} = c^{\mathrm{o,b}}_{\mathrm{TB}}$ and $c^{\mathrm{w,b}} = c^{\mathrm{w,b}}_{\mathrm{HCit}}$ are the electrolyte concentrations in the bulk organic and aqueous phases, and $f = F/RT$. The pH in the bulk aqueous phase determines the H^+ concentration $c^{\mathrm{w,b}}_{\mathrm{H}}$, and $c^{\mathrm{w,b}}_{\mathrm{Li}} = 2c^{\mathrm{w,b}} - c^{\mathrm{w,b}}_{\mathrm{H}}$. The chemical partition coefficients P_i of the ions are related to their standard transfer potentials and to the Gibbs free energies of transfer,

$$RT\ln P_{\mathrm{R_2N}} = F\Delta^{\mathrm{IN}}_{\mathrm{o}}\phi^{\circ}_{\mathrm{R_2N}} = \mu^{\circ,\mathrm{o}}_{\mathrm{R_2N}} - \mu^{\circ,\mathrm{IN}}_{\mathrm{R_2N}} \quad \text{(S6)}$$

$$RT\ln P_{\mathrm{TB}} = -F\Delta^{\mathrm{IN}}_{\mathrm{o}}\phi^{\circ}_{\mathrm{TB}} = \mu^{\circ,\mathrm{o}}_{\mathrm{TB}} - \mu^{\circ,\mathrm{IN}}_{\mathrm{TB}} \quad \text{(S7)}$$

$$RT\ln P_{\mathrm{HCit}} = 2F\Delta^{\mathrm{w}}_{\mathrm{IN}}\phi^{\circ}_{\mathrm{HCit}} = \mu^{\circ,\mathrm{w}}_{\mathrm{HCit}} - \mu^{\circ,\mathrm{IN}}_{\mathrm{HCit}} \quad \text{(S8)}$$

$$RT\ln P_{\mathrm{H}} = -F\Delta^{\mathrm{w}}_{\mathrm{IN}}\phi^{\circ}_{\mathrm{H}} = \mu^{\circ,\mathrm{w}}_{\mathrm{H}} - \mu^{\circ,\mathrm{IN}}_{\mathrm{H}} \quad \text{(S9)}$$

$$RT\ln P_{\mathrm{Li}} = -F\Delta^{\mathrm{w}}_{\mathrm{IN}}\phi^{\circ}_{\mathrm{Li}} = \mu^{\circ,\mathrm{w}}_{\mathrm{Li}} - \mu^{\circ,\mathrm{IN}}_{\mathrm{Li}} \quad \text{(S10)}$$

where $\mu_i^{\circ,\varphi}$ is the standard chemical potential of ionic species *i* in phase φ.

The ion exchange reaction, Equation (7), main text, can be considered as the combination of the acid dissociation

$$-\mathrm{COOH(IN)} \rightleftarrows -\mathrm{COO^-(IN)} + \mathrm{H^+(IN)} \quad \text{(S11)}$$

and the binding or adsorption reaction

$$-\mathrm{COO^-(IN)} + \mathrm{R_2N^+(IN)} \rightleftarrows -\mathrm{COOR_2N(IN)}\,. \quad \text{(S12)}$$

Hence, the ion exchange equilibrium constant can be considered the product of the acid dissociation constant $K^{\mathrm{IN}}_{\mathrm{a}}$ and the R_2N^+ binding constant $K^{\mathrm{IN}}_{\mathrm{b}}$,

$$K_{\mathrm{IE}}^{\circ,\mathrm{IN}} = K_{\mathrm{a}}^{\mathrm{IN}} K_{\mathrm{b}}^{\mathrm{IN}} c^{\circ}. \tag{S13}$$

These constants are defined by the standard reaction Gibbs energies,

$$\Delta G_{\mathrm{IE}}^{\circ,\mathrm{IN}} = -RT\ln K_{\mathrm{IE}}^{\circ,\mathrm{IN}} = \mu_{\mathrm{COOR_2N}}^{\circ} + \mu_{\mathrm{H}}^{\circ,\mathrm{IN}} - \mu_{\mathrm{COOH}}^{\circ} - \mu_{\mathrm{R_2N}}^{\circ,\mathrm{IN}} \tag{S14}$$

$$\Delta G_{\mathrm{a}}^{\circ,\mathrm{IN}} = -RT\ln K_{\mathrm{a}}^{\mathrm{IN}} = \mu_{\mathrm{COO^-}}^{\circ} + \mu_{\mathrm{H}}^{\circ,\mathrm{IN}} - \mu_{\mathrm{COOH}}^{\circ} \tag{S15}$$

$$\Delta G_{\mathrm{b}}^{\circ,\mathrm{IN}} = -RT\ln K_{\mathrm{b}}^{\mathrm{IN}} = \mu_{\mathrm{COOR_2N}}^{\circ} - \mu_{\mathrm{COO^-}}^{\circ} - \mu_{\mathrm{R_2N}}^{\circ,\mathrm{IN}} \quad . \tag{S16}$$

Using the above equilibrium conditions, the electroneutrality condition (Equation (2), main text) can be written as an equation in the variable $y = \mathrm{e}^{f\Delta_{\mathrm{IN}}^{\mathrm{w}}\phi}$,

$$\frac{K_{\mathrm{a}}^{\mathrm{IN}} c^{\circ} c_{\mathrm{T,COO}}}{K_{\mathrm{a}}^{\mathrm{IN}} c^{\circ} + \left(c_{\mathrm{H}}^{\mathrm{w,b}} P_{\mathrm{H}} + K_{\mathrm{IE}}^{\circ,\mathrm{IN}} c^{\mathrm{o,b}} P_{\mathrm{R_2N}} \mathrm{e}^{-f\Delta_{\mathrm{o}}^{\mathrm{w}}\phi}\right) y} = 2c^{\mathrm{w,b}}(P_{\mathrm{Li}} y - P_{\mathrm{HCit}} y^{-2})$$
$$+ c^{\mathrm{o,b}}\left(P_{\mathrm{R_2N}} \mathrm{e}^{-f\Delta_{\mathrm{o}}^{\mathrm{w}}\phi} y - P_{\mathrm{TB}} \mathrm{e}^{f\Delta_{\mathrm{o}}^{\mathrm{w}}\phi} y^{-1}\right) + c_{\mathrm{H}}^{\mathrm{w,b}}(P_{\mathrm{H}} - P_{\mathrm{Li}}) y \tag{S17}$$

whose numerical solution allows the determination of the potential drop $\Delta_{\mathrm{IN}}^{\mathrm{w}}\phi = (RT/F)\ln y$. In the case of negligible $c_{\mathrm{COO^-}}^{\mathrm{IN}}$ and very negative $\Delta_{\mathrm{o}}^{\mathrm{w}}\phi$, Equation (S17) reduces to $2c_{\mathrm{HCit}}^{\mathrm{IN}} = c_{\mathrm{R_2N}}^{\mathrm{IN}}$, *i.e.*, $2c^{\mathrm{w,b}} P_{\mathrm{HCit}} y^{-2} = c^{\mathrm{o,b}} P_{\mathrm{R_2N}} \mathrm{e}^{-f\Delta_{\mathrm{o}}^{\mathrm{w}}\phi} y$, which provides a convenient initial guess

$$y_0 = \mathrm{e}^{f\Delta_{\mathrm{o}}^{\mathrm{w}}\phi/3} \left(\frac{2c^{\mathrm{w,b}} P_{\mathrm{HCit}}}{c^{\mathrm{o,b}} P_{\mathrm{R_2N}}}\right)^{1/3} \tag{S18}$$

to solve Equation (S17). That is, $\Delta_{\mathrm{IN}}^{\mathrm{w}}\phi$ is then close to one third of $\Delta_{\mathrm{o}}^{\mathrm{w}}\phi$.

S3.2 Simulating CVs

The CVs can be simulated using an equivalent electrical circuit consisting of the solution resistance R_{sol} in series with the parallel combination of the film capacitance *C* and the charge transfer resistance R_{ct}. The potential applied to this equivalent circuit during a CV scan is

$$\Delta_{\mathrm{o}}^{\mathrm{w}}\phi(t) = \varepsilon_{\mathrm{f}} + \nu\,|t_{\max} - t|, \quad (0 \le t \le 2t_{\max}) \tag{S19}$$

where $t_{\max} = (\varepsilon_{\mathrm{i}} - \varepsilon_{\mathrm{f}})/\nu$ and ν is the scan rate ($\nu = -\mathrm{d}\Delta_{\mathrm{o}}^{\mathrm{w}}\phi/\mathrm{d}t$ for $0 \le t \le t_{\max}$). The potential drop across *C* and R_{ct} is denoted as $\varepsilon_{\mathrm{c}}(t)$. Note that *C* is a function of this potential, Equation (10), main text. The sum of the current $\varepsilon_{\mathrm{c}}(t)/R_{\mathrm{ct}}$ across R_{ct} and the pseudo-capacitive current $\mathrm{d}q^{\mathrm{o}}/\mathrm{d}t = C\mathrm{d}\varepsilon_{\mathrm{c}}/\mathrm{d}t$ across *C* is the observed current density $j(t) = (\Delta_{\mathrm{o}}^{\mathrm{w}}\phi - \varepsilon_{\mathrm{c}})/R_{\mathrm{sol}}$,

$$\frac{\Delta_{\mathrm{o}}^{\mathrm{w}}\phi(t) - \varepsilon_{\mathrm{c}}(t)}{R_{\mathrm{sol}}} = \frac{\varepsilon_{\mathrm{c}}(t)}{R_{\mathrm{ct}}} + C(\varepsilon_{\mathrm{c}}(t))\frac{\mathrm{d}\varepsilon_{\mathrm{c}}}{\mathrm{d}t}\,. \tag{S20}$$

The solution of this equation in $\varepsilon_{\mathrm{c}}(t)$, with the initial condition $\varepsilon_{\mathrm{c}}(0) = \varepsilon_{\mathrm{i}}$, allows us to evaluate $j(t)$. The key feature of these CVs is the "adsorption" current $j \approx \mathrm{d}q^{\mathrm{o}}/\mathrm{d}t \approx C\nu$. The

small difference in the peak potentials of the forward and backward scans is mainly determined by R_{sol}.

S3.3 Frumkin binding isotherm

The equilibrium condition for the R_2N^+ adsorption reaction (S12) is $\mu_{\mathrm{COOR_2N}} = \mu_{\mathrm{COO^-}} + \mu^{\mathrm{IN}}_{\mathrm{R_2N}}$ and can also be presented as

$$\frac{c_{\mathrm{COOR_2N}}}{c_{\mathrm{COOH}}+c_{\mathrm{COO^-}}} = \frac{\theta}{1-\theta} = \frac{K^{\circ,\mathrm{IN}}_{\mathrm{IE}} c^{\mathrm{IN}}_{\mathrm{R_2N}}}{K^{\mathrm{IN}}_{\mathrm{a}} c^{\circ} + c^{\mathrm{IN}}_{\mathrm{H}}} \tag{S21}$$

$$\frac{c_{\mathrm{COOR_2N}}}{c_{\mathrm{COO^-}}} = \frac{\theta}{1-\theta}\frac{1}{\alpha} = K^{\mathrm{IN}}_{\mathrm{b}} c^{\mathrm{IN}}_{\mathrm{R_2N}} \tag{S22}$$

where $\theta = c_{\mathrm{COOR_2N}}/c_{\mathrm{T,COO}}$ is the fraction of sites occupied by R_2N^+ ions, α is the degree of acid dissociation defined by $\alpha/(1-\alpha) = c_{\mathrm{COO^-}}/c_{\mathrm{COOH}}$, and we have used Equations (6), main text, and (S13). When the species –$COOR_2N$ interact, their chemical potential is

$$\mu_{\mathrm{COOR_2N}} = \mu^{\circ}_{\mathrm{COOR_2N}} + RT\ln\theta + gRT\theta, \tag{S23}$$

and the Frumkin isotherm

$$\frac{\theta}{1-\theta}\mathrm{e}^{g\theta} = \alpha K^{\mathrm{IN}}_{\mathrm{b}} c^{\mathrm{IN}}_{\mathrm{R_2N}} = \frac{K^{\circ,\mathrm{IN}}_{\mathrm{IE}} c^{\mathrm{IN}}_{\mathrm{R_2N}}}{K^{\mathrm{IN}}_{\mathrm{a}} c^{\circ} + c^{\mathrm{IN}}_{\mathrm{H}}} = \frac{K^{\circ,\mathrm{IN}}_{\mathrm{IE}} c^{\mathrm{o,b}} P_{\mathrm{R_2N}} \mathrm{e}^{-f\Delta^{\mathrm{W}}_{\mathrm{o}}\phi} \mathrm{e}^{f\Delta^{\mathrm{W}}_{\mathrm{IN}}\phi}}{K^{\mathrm{IN}}_{\mathrm{a}} c^{\circ} + c^{\mathrm{w,b}}_{\mathrm{H}} P_{\mathrm{H}} \mathrm{e}^{f\Delta^{\mathrm{W}}_{\mathrm{IN}}\phi}} \tag{S24}$$

should then be used to describe the cooperative adsorption of R_2N^+ ions, *i.e.*, the equilibrium of reaction (S12).

Using a lattice model and the mean-field approximation, the interaction energy between adsorbed R_2N^+ ions is estimated as $E = (1/2)z_{\mathrm{c}}\varepsilon N^2/N_{\mathrm{s}}$, where N_{s} is the number of lattice sites, z_{c} is the coordination number (*i.e.*, the number of nearest neighbours), N is the number of adsorbed ions, and ε is the molar interaction energy between ions adsorbed in neighbouring sites. Thence, the chemical potential of species –$COOR_2N$ is given by Equation (S23). Negative values of $g = z_{\mathrm{c}}\varepsilon/RT$ correspond to attractive interactions between adsorbed ions, which reduce $\mu_{\mathrm{COOR_2N}}$, and to positive cooperativity. When $g \leq -4$, *i.e.*, for temperatures below the critical one, $T_{\mathrm{c}} = -z_{\mathrm{c}}\varepsilon/4R > 0$, phase transitions can occur and to avoid unrealistic predictions, the grand canonical ensemble should then be used to deduce the adsorption isotherm.[4]

If the Frumkin adsorption model is used then $K_{\mathrm{IE}}^{\circ,\mathrm{IN}}\mathrm{e}^{-g\theta}$ should replace $K_{\mathrm{IE}}^{\circ,\mathrm{IN}}$ in Equations (8), (9) and (11) in the main text. For instance, Equation (9) becomes

$$\frac{c_{\mathrm{COO^-}}}{c_{\mathrm{T,COO}}} = \frac{K_{\mathrm{a}}^{\mathrm{IN}} c^{\circ}}{K_{\mathrm{a}}^{\mathrm{IN}} c^{\circ} + c_{\mathrm{H}}^{\mathrm{IN}} + K_{\mathrm{IE}}^{\circ,\mathrm{IN}}\mathrm{e}^{-g\theta} c_{\mathrm{R_2N}}^{\mathrm{IN}}} \,. \tag{S25}$$

The system formed by Equations (S24) and (S17), with $K_{\mathrm{IE}}^{\circ,\mathrm{IN}}\mathrm{e}^{-g\theta}$ replacing $K_{\mathrm{IE}}^{\circ,\mathrm{IN}}$ in the latter, must be simultaneously solved to determine the unknowns $\Delta_{\mathrm{IN}}^{\mathrm{w}}\phi$ and θ as functions of $\Delta_{\mathrm{o}}^{\mathrm{w}}\phi$, for given values of $c^{\mathrm{o,b}}$, $c^{\mathrm{w,b}}$ and $c_{\mathrm{H}}^{\mathrm{w,b}}$. Then, the capacitance *C* is calculated with Equation (10), main text, and the CV is simulated with Equation (S20).

S3.4 Relations between the equilibrium constants in different phases

The equilibrium constant of the acid-dissociation reaction

$$-\mathrm{COOH(IN)} \rightleftarrows -\mathrm{COO^-(IN)} + \mathrm{H^+(w)} \tag{S26}$$

is the acidity constant $K_{\mathrm{a}} = 10^{-5.8}$, and the standard Gibbs energy of reaction is

$$\Delta G_{\mathrm{a}}^{\circ} = -RT\ln K_{\mathrm{a}} = \mu_{\mathrm{COO^-}}^{\circ} + \mu_{\mathrm{H^+}}^{\circ,\mathrm{w}} - \mu_{\mathrm{COOH}}^{\circ} \,. \tag{S27}$$

The equilibrium constant of the binding reaction

$$-\mathrm{COO^-(IN)} + \mathrm{R_2N^+(o)} \rightleftarrows -\mathrm{COOR_2N(IN)} \tag{S28}$$

is the (intrinsic) binding constant K_{b} which is implicitly defined as

$$\Delta G_{\mathrm{b}}^{\circ} = -RT\ln K_{\mathrm{b}} = \mu_{\mathrm{COOR_2N}}^{\circ} - \mu_{\mathrm{COO^-}}^{\circ} - \mu_{\mathrm{R_2N}}^{\circ,\mathrm{o}} \,. \tag{S29}$$

The equilibrium constant of the ion exchange reaction

$$-\mathrm{COOH(IN)} + \mathrm{R_2N^+(o)} \rightleftarrows -\mathrm{COOR_2N(IN)} + \mathrm{H^+(w)} \tag{S30}$$

is the (intrinsic) ion exchange constant K_{IE}° which is implicitly defined as

$$\Delta G_{\mathrm{IE}}^{\circ} = -RT\ln K_{\mathrm{IE}}^{\circ} = \mu_{\mathrm{COOR_2N}}^{\circ} + \mu_{\mathrm{H}}^{\circ,\mathrm{w}} - \mu_{\mathrm{COOH}}^{\circ} - \mu_{\mathrm{R_2N}}^{\circ,\mathrm{o}} \,. \tag{S31}$$

Its relation with the acidity and the binding constants is $K_{\mathrm{IE}}^{\circ} = K_{\mathrm{a}} K_{\mathrm{b}} c^{\circ}$.

Similarly, in the ZnPor-IN film (phase IN), the equilibrium constant of reaction (S11) is

$$K_{\mathrm{a}}^{\mathrm{IN}} = K_{\mathrm{a}} P_{\mathrm{H}} \,. \tag{S32}$$

The equilibrium constant of reaction (S12) is defined through Eq. (S16) and its relation to that in bulk phase is

$$K_{\mathrm{b}}^{\mathrm{IN}} = K_{\mathrm{b}} / P_{\mathrm{R_2N}} \,. \tag{S33}$$

The equilibrium constant of the ion exchange reaction in the film, Equation (7) in the main text, is defined through Eq. (S14) and its relation to that in bulk phase is $K_{\mathrm{IE}}^{\circ,\mathrm{IN}} = K_{\mathrm{a}}^{\mathrm{IN}} K_{\mathrm{b}}^{\mathrm{IN}} c^{\circ} = K_{\mathrm{IE}}^{\circ} P_{\mathrm{H}} / P_{\mathrm{R_2N}}$. That is, the solvation effects on ion partitioning also affect the binding constant and the ion exchange equilibrium constant.

S3.5 Mathematica code to simulate the CVs in the presence of the ZnPor-IN film

Files available free of charge on the ACS Publications website.

Table S3. Parameter values for the simulated CVs in Figure 3a, main text. The chemical partition coefficient is $P_i = 3 \times 10^{-4}$ for all ionic species (i = R_2N^+, TB^-, $HCit^{2-}$, H^+, Li^+) and $\mathrm{p}K_{\mathrm{b}} = -\lg K_{\mathrm{b}} = -\lg\left(K_{\mathrm{b}}^{\mathrm{IN}} P_{\mathrm{R_2N}}\right)$.

Γ_{ZnPor} /(nmol·cm^{-2})	$c_{\mathrm{T,COO}}$/mM	pK_{b}	R_{sol}/(kΩ·cm^2)	R_{ct}/(MΩ·cm^2)
0.34	42	3.3	4.5	3.5
0.88	100	3.3	4.5	2.0
1.94	214	3.1	2.8	2.0
4.19	416	3.1	1.4	2.0

Table S4. Parameter values for the simulated CVs in Figures 3b and c, main text. As shown in Table S3, $c_{\mathrm{T,COO}}$ = 42 mM because Γ_{ZnPor} = 0.34 nmol·cm^{-2}. The chemical partition coefficient is $P_i = 3 \times 10^{-4}$ for all ionic species (i = R_2N^+, TB^-, $HCit^{2-}$, H^+, Li^+).

pH	$c^{\mathrm{o,b}}$/mM	pK_{b}	R_{sol}/(kΩ·cm^2)	R_{ct}/(MΩ·cm^2)
5.8	5.0	3.50	4.0	3.0
5.0	5.0	3.55	4.0	3.5
4.5	5.0	3.65	4.0	2.5
4.0	5.0	3.65	4.0	2.5
3.0	5.0	3.65	4.0	2.5
5.8	5.0	3.60	2.8	3.0
5.8	2.5	3.40	2.8	3.0
5.8	1.0	3.60	2.8	3.0

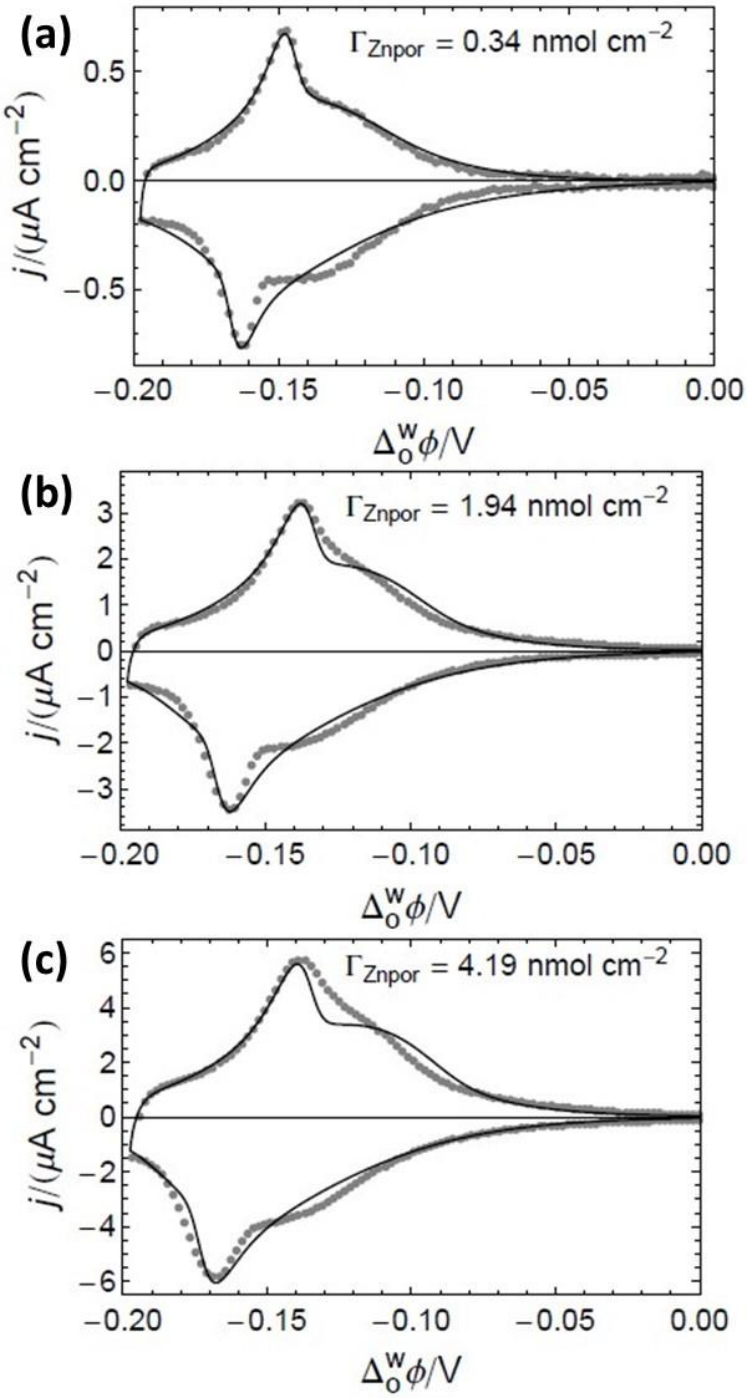

Figure S8. The consideration of two types of binding sites, described by Equation (S24) with $g_{\mathrm{narrow}} = -3.5$ and $g_{\mathrm{broad}} = -0.7$, predicts simulated CVs (lines) at 1 mV·s^{-1} that resemble more closely the experimental observations (symbols). Comparisons are provided for CVs obtained with Γ_{ZnPor} values of 0.34, 1.94 and 4.19 nmol·cm^{-2}. The parameter values (see Table S5) have been chosen on the basis of a qualitative agreement and not using a fitting algorithm.

Table S5. Parameter values for the simulated CVs in Figures 4, main text, and S7. The partition coefficient is $P_i = 3 \times 10^{-5}$ for all ionic species (i = R_2N^+, TB^-, $HCit^{2-}$, H^+, Li^+). The values of $pK_b = -\lg K_b = -\lg\left(K_b^{IN} P_{R_2N}\right)$ are shown. The carboxyl groups responsible for the narrow peak have a more negative Frumkin parameter $g_{narrow} = -3.5$ and a smaller binding constant $K_{b,narrow}$, so that the narrow peak appears at more negative $\Delta_o^w \phi$, compared to the broad peak with $g_{broad} = -0.7$ and larger $K_{b,broad}$.

Γ_{ZnPor} /(nmol·cm^{-2})	$c_{T,COO}^{narrow}$/mM	$c_{T,COO}^{broad}$/mM	pK_b^{narrow}	pK_b^{broad}	R_{sol}/(kΩ·cm^2)	R_{ct}/(MΩ·cm^2)
0.34	10	31	4.04	3.30	13	7
0.88	24	70	4.13	3.40	8	5
1.94	46	160	3.98	3.20	5.4	4
4.19	84	295	4.05	3.20	3.7	10

Section S4. The kinetics of structural changes in the ZnPor-IN film during electrochemically-driven reversible ion intercalation

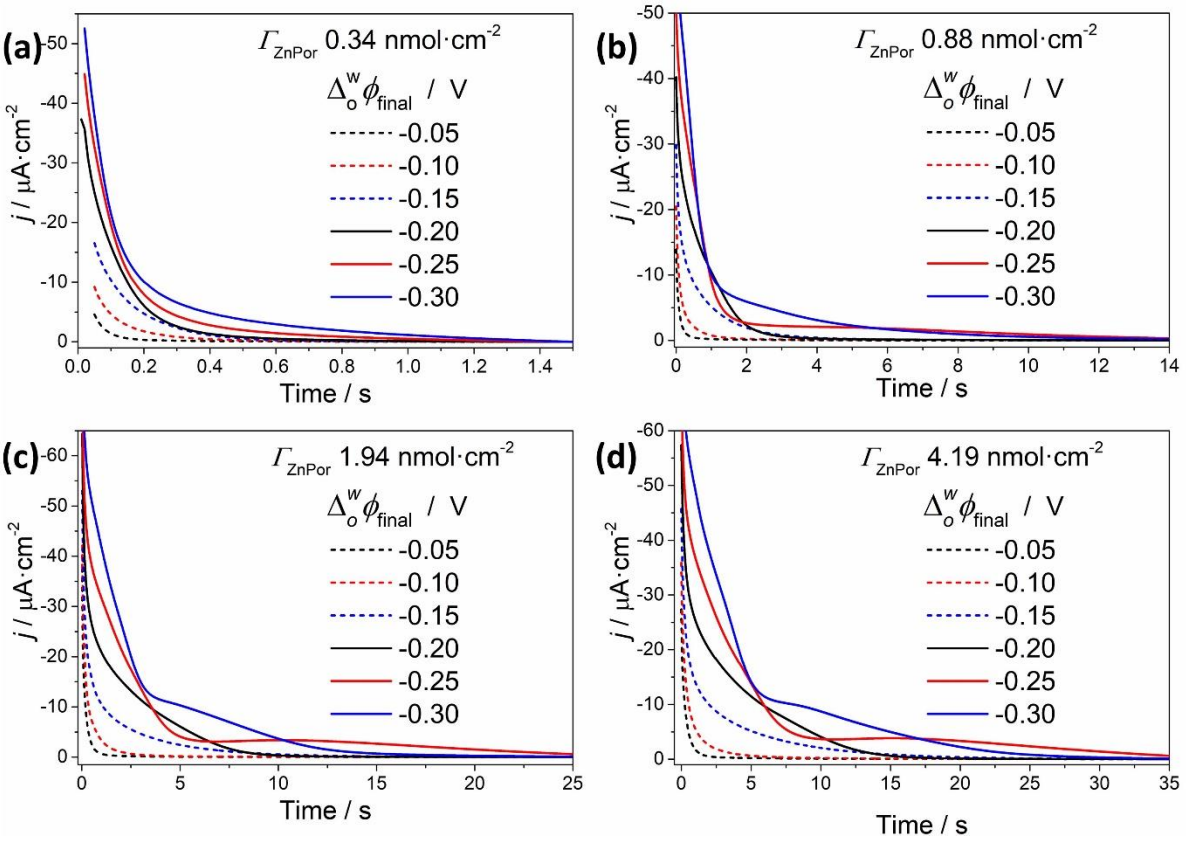

Figure S9. Current transients probing the influence of $\Delta_o^w\phi_{final}$ were obtained by varying $\Delta_o^w\phi_{final}$ in 50 mV increments at a constant $\Delta_o^w\phi_{initial}$ of +0.25 V for 30 s ($t_{initial}$) with Γ_{ZnPor} values of **(a)** 0.34, **(b)** 0.88, **(c)** 1.94 and **(d)** 4.19 nmol·cm^{-2}, respectively.

Table S6. All t_{max} values in Table S6 were obtained from the derivative of current transients obtained in the presence of the ZnPor-IN film as a function of both Γ_{ZnPor} and $\Delta_o^w\phi_{initial}$ with a constant $\Delta_o^w\phi_{initial}$ of +0.25 V for 30 s ($t_{initial}$).

Γ_{ZnPor}/(nmol·cm^{-2})	t_{max1}/s			t_{max2}/s			t_{max3}/s		
	–0.25 V	–0.30 V	–0.35 V	–0.25 V	–0.30 V	–0.35 V	–0.25 V	–0.30 V	–0.35 V
0.34	0.43	0.27	-	-	0.51	0.50	-	-	-
0.88	0.75	0.08	1.31	-	0.33	3.29	-	1.71	-
1.94	1.03	0.7	0.66	2.87	1.73	1.3	-	10.22	4.5
4.19	1.81	1.14	0.85	4.86	2.82	2.1	-	15.21	8.13

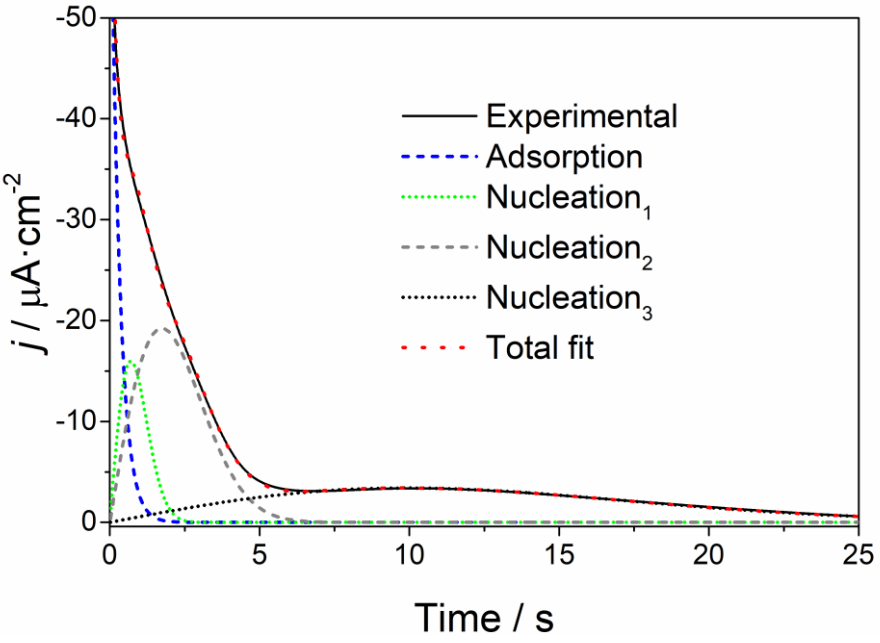

Figure S10. Using the t_{max} values outlined in Table S6 obtained from the derivative of each current transient, the total fitted current for any transient may be obtained as a summation of the adsorption and three nucleation components using exponential decay and Gaussian-type functions, respectively. In this example, the current transient fitted (dotted red line) is that obtained experimentally (solid black line) with a Γ_{ZnPor} of 1.94 nmol·cm^{-2}, $\Delta_o^w\phi_{initial}$ of +0.25 V for 30 s, and $\Delta_o^w\phi_{final}$ of –0.25 V.

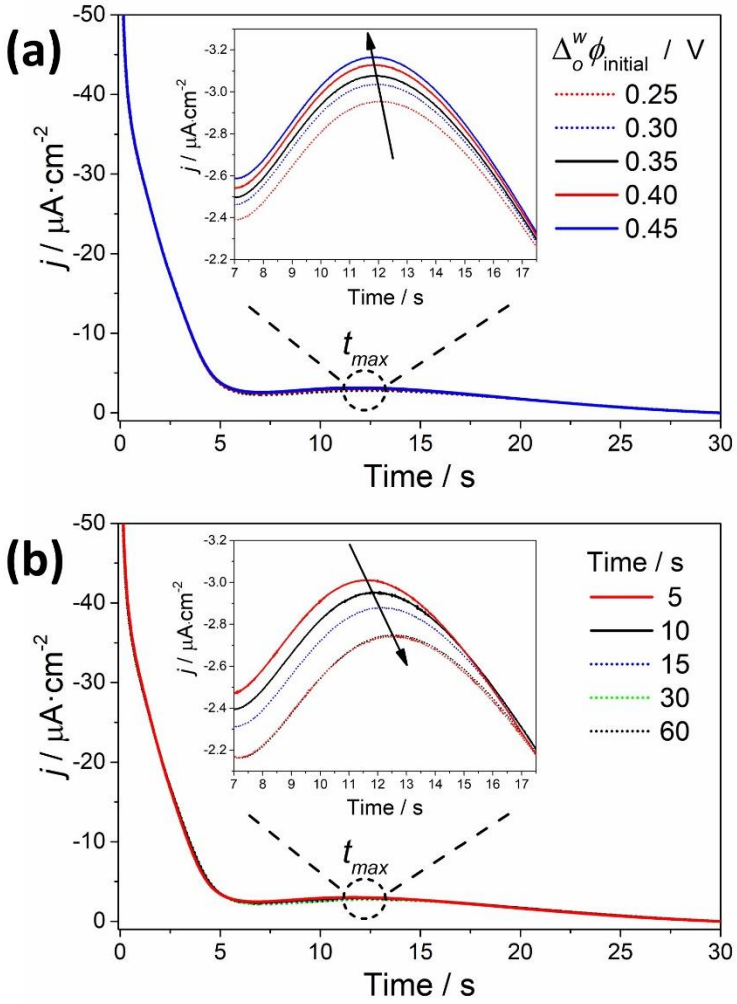

Figure S11. (a) Current transients probing the influence of $\Delta_o^w\phi_{initial}$ were obtained at a constant $t_{initital}$ of 30 s, Γ_{ZnPor} of 4.19 nmol·cm^{-2}, and $\Delta_o^w\phi_{final}$ of –0.25 V. **(b)** Current transients probing the influence of $t_{initial}$ were obtained at a constant Γ_{ZnPor} of 4.19 nmol·cm^{-2}, $\Delta_o^w\phi_{initial}$ of +0.25 V, and $\Delta_o^w\phi_{final}$ of –0.25 V.

Supporting References

(1) Molina-Osorio, A. F.; Cheung, D.; O'Dwyer, C.; Stewart, A. A.; Dossot, M.; Herzog, G.; Scanlon, M. D. Self-Assembly of Porphyrin Nanostructures at the Interface between Two Immiscible Liquids. *J. Phys. Chem. C* **2020**, *124* (12), 6929–6937. https://doi.org/10.1021/acs.jpcc.0c00437.

(2) Smirnov, E.; Peljo, P.; Scanlon, M. D.; Girault, H. H. Gold Nanofilm Redox Catalysis for Oxygen Reduction at Soft Interfaces. *Electrochim. Acta* **2016**, *197*, 362–373. https://doi.org/10.1016/j.electacta.2015.10.104.

(3) Cherian, S.; Wamser, C. C. Adsorption and Photoactivity of Tetra(4-Carboxyphenyl)Porphyrin (TCPP) on Nanoparticulate TiO_2. *J. Phys. Chem. B* **2000**, *104* (15), 3624–3629. https://doi.org/10.1021/jp994459v.

(4) Cervera, J.; Gilabert, M. A.; Manzanares, J. A. Liquid-Vapor Coexistence and the PVT Surface of a Lattice Fluid. *Am. J. Phys.* **2011**, *79* (2), 206–213. https://doi.org/10.1119/1.3531942.